sciendo

Civil and Environmental Engineering
Vol. 21, Issue 2, 1384-1401, DOI: 10.2478/cee-2025-0101

EXPERIMENTAL ASSESSMENT OF DURABILITY IN 3D PRINTED CEMENTITIOUS MATERIALS

Karel HURTIG[1], David ČÍTEK[1,*], Milan HOLÝ[1], Peter KOTEŠ[2], Adam ČÍTEK[1]

[1] Klokner Institute, Czech Technical University in Prague, 166 08 Prague, Czech Republic.
[2] University of Zilina, Faculty of Civil Engineering, Univerzitná 8215, 010 26 Žilina, Slovakia.
[*] corresponding author: david.citek@cvut.cz

Abstract

The development of additive technologies in construction, particularly 3D printing of cement-based composites, places increased demands on verifying the long-term durability of the resulting material under real exposure conditions. The presented study focuses on the experimental evaluation of selected durability parameters of a cementitious composite designed for 3D printing, with particular attention paid to the effect of a setting accelerator and the presence of dispersed steel reinforcement. The performed tests included the assessment of surface resistance to water and chemical de-icing agents, freeze–thaw resistance, water absorption, depth of water penetration under pressure, and carbonation depth after long-term exposure to outdoor environmental conditions. The results reveal significant differences in durability performance depending on the mixture composition. The study also highlights the specific aspects of durability behaviour arising from the layered structure of the material produced by the 3D printing process.

Keywords:

3D concrete printing;
Durability;
Freeze-thaw resistance;
Carbonation;
Fibre reinforcement.

1 Introduction

Additive manufacturing of concrete, commonly known as 3D concrete printing (3DCP), has rapidly emerged as an innovative construction technique offering significant advantages. By extruding cementitious “ink” layer by layer, 3DCP eliminates the need for formwork and enables the creation of complex geometries with greater efficiency and reduced waste. Early studies estimate that printing can cut construction waste by over 50% and substantially reduce labor and time requirements. This technology aligns with sustainable construction goals and has been successfully demonstrated in applications from building components to infrastructure (e.g. walls, bridge elements, artificial reefs) where design flexibility is desired. However, alongside these benefits, ensuring the structural durability of 3D printed cementitious materials has become a critical concern. Unlike conventionally cast concrete, which benefits from formwork and often vibration compaction, 3D printed elements are built freeform and exposed directly to environmental conditions from an early age. As a result, questions remain about their long-term performance under aggressive conditions, and current construction codes lack specific provisions to assess 3D-printed concrete’s long-term behaviour. This motivates research into durability issues, since the viability of 3D printed structural components hinges not only on initial mechanical properties but also on their ability to resist deterioration over decades of service.

The durability of 3D-printed concrete is governed by the ingress of aggressive agents (water, ions) into its porous structure and the ensuing degradation processes. Water acts as a carrier for chloride ions and CO_2, which can penetrate the concrete and chemically react with hydration products, disrupting the structure and reducing the concrete’s alkalinity (carbonation). These processes diminish reinforcement passivation and accelerate corrosion, thereby shortening the service life of the structure. Cyclic freezing and thawing (F-T) meanwhile generates expansive pressures in water-saturated pores, leading to microcracking, surface scaling, and a gradual loss of strength [1]. Conventional cast concrete benefits from vibration during placement, producing a denser and more homogeneous structure with fewer weak points. By contrast, 3D-printed concrete is not vibrated and is formed by the successive extrusion of layers, which results in pronounced anisotropy and the formation of interlayer interfaces [1]. These interfacial zones represent weak regions and increase vulnerability to degradation. 3DPC exhibits higher overall porosity, weaker interlayer bonding, and directionally oriented cracks, especially under freeze–thaw loading [1], [8]. In addition, the absence of formwork exposes freshly printed concrete to

the environment, causing greater plastic and drying shrinkage and early cracking that can serve as pathways for the ingress of harmful substances [2]. Taken together, relative to conventional concrete, 3DPC generally shows lower resistance to chloride penetration, faster carbonation progress, and increased sensitivity to freeze–thaw action.

A defining feature of 3DPC is the interlayer zone, which strongly affects the material's transport properties. The 3D-printing process introduces more pores and air voids. These pores occur both within filaments (intra-) and between layers (inter-), and their volume increases with longer time gaps between deposited layers. At interlayer interfaces, elongated, interconnected pores oriented along the print direction have been observed; these are practically absent in conventional concrete [2], [8]. This irregular and continuous porous network within the interface creates preferential pathways for the movement of water and ions. X-ray computed tomography (X-CT) experiments confirm that water propagates along interlayer interfaces faster than through the homogeneous bulk of reference cast concrete [3]. For example, using in-situ X-CT with CsCl as a tracer, [3] showed that the rate of capillary absorption parallel to the layers in 3DPC significantly exceeds both the rate across the layers and the rate in conventional concrete. Capillary absorption coefficients in directions T1, T2, T3 (aligned with layer orientation) exhibit marked anisotropy The highest absorption is parallel to the layers and the lowest is perpendicular to them [3]. Consequently, resistance to the ingress of water and dissolved aggressive media in 3DPC is direction-dependent and poorest in the plane of the interlayer interfaces. These findings align with microstructural observations. Pores near the interface in printed concrete are more interconnected and more concentrated than in the core of a layer. Van Der Putten et al. [2] also report that with zero interlayer delay, ingress is relatively uniform; even so, the total ingress in printed specimens is higher than in cast concrete. With longer delays, significantly deeper penetration occurs along the interfaces due to the higher porosity of these zones [2].

Available studies indicate that 3D-printed concrete is more susceptible to the ingress of chloride ions and CO_2 compared to conventionally compacted concrete. Printed specimens generally exhibit lower resistance to chlorides, reflected in higher chloride migration rates and greater penetration depths. The main reason is the presence of interconnected, elongated voids at filament and layer interfaces that facilitate ion transport [4]. For instance, the non-steady-state chloride diffusion coefficient in 3DPC is often higher than in vibrated concrete, confirming faster chloride transport through the structure [4]. In some cases, chloride penetration depth in printed concrete is reported to be tens of percent greater than in reference specimens. Ler et al. [4] summarize that chloride ingress in 3DPC exceeds that of conventional concrete unless special measures are taken, and that increasing layer height or interlayer delay further degrades chloride resistance. A similar trend holds for carbonation. Conventional vibrated concrete shows a smaller depth of carbonated zone than 3DPC, particularly in the interlayer regions of printed concrete [4]. Interlayer zones in 3DPC typically carbonate faster and deeper due to higher local permeability and possible microcracking. It has been observed that interlayer delay (the time gap between layer depositions) accelerates carbonation at the interface The longer interval allows microcrack formation and drying, which increase CO_2 permeability [4]. As a result, over time the carbonation depth through the interfaces can approach that of the filaments' exposed surfaces. In summary, conventional concrete generally exhibits higher resistance to both chloride ingress and carbonation, whereas 3DPC requires mitigating measures to avoid a faster depletion of the alkaline reserve and reduced durability [2].

The behaviour of 3DPC under freeze–thaw cycling shows certain differences from conventional concrete [10]. Freeze–thaw cycles generate ice in pores and associated stresses that can damage the material. In 3D-printed concrete, these processes can be affected by anisotropic microstructure and interlayer interfaces. Some studies suggest that printed and cast concretes can have comparable frost resistance in the early stages of degradation testing. For example, Van Der Putten et al. (2022) [2] found no significant difference after 14 F-T cycles between printed and vibrated specimens, attributing this to the higher content of air voids in printed concrete acting as relief spaces for ice [2]. All of their 3DPC specimens even showed very good frost resistance, with a maximum mass loss of only ~0.18% and minimal strength reduction after 300 freeze-thaw cycles. This suggests that the printing process itself can introduce a greater share of entrapped air voids (pore sizes > 75 μm) which, similarly to intentionally air-entrained concrete, relieve ice pressure [1]. At the same time, however, interlayer interfaces are critical locations where frost action is more severe. When specimens are oriented perpendicular to the layers, F–T cycles tend to initiate cracking along the horizontal interfaces, which are less cohesive and contain more voids [1]. Faster deterioration has also been observed on exposed layered surfaces. Cracks typically propagate along the interface and can cause layer spalling [1]. This phenomenon is particularly pronounced in printed elements exposed horizontally to freezing (e.g., slabs), where

weakened planes between layers allow the cover concrete to delaminate more easily. Besides freezing, resistance to de-icing salts (salt scaling) is also examined. In freeze-thaw tests with saline solution, concrete additionally suffers from salt crystallization in pores, producing further expansive forces. In 3D-printed concretes, surface scaling due to salts can be more pronounced because the capillary network in the surface zone is more connected, enabling deeper penetration of the saline solution. Ler et al. (2024) [4] note that using a saline solution in F-T testing imposes additional stress on pore walls from crystallizing salt hydrates, which, in a higher-porosity material like 3DPC, can accelerate degradation. Overall, ensuring frost resistance in 3DPC is essential. For example, through proper air-entrainment or other mix adjustments, otherwise premature surface damage (scaling) and cracking, especially along interlayer planes, may occur.

The above findings indicate that achieving durable 3D-printed concrete requires targeted adjustments to both mixture composition and production process. Mix optimization primarily involves the use of suitable binders and supplementary materials to densify the microstructure. To limit ingress, increasing the share of supplementary cementitious materials (SCMs) such as slag, fly ash, or silica fume has proven effective. These fine additions fill pores and refine capillaries, thereby reducing permeability [5], [8], [9]. In chloride-rich environments, SCMs have been shown to reduce chloride penetration depth by tens of percent; in one study, an optimized printable mix with a high SCM content even exhibited 70-83% lower chloride penetration depth than a conventional reference [5]. Fiber reinforcement is another effective measure. Adding polymer fibres (e.g., polyvinyl alcohol, PVA) at about 0.5% by volume improves 3DPC toughness and crack resistance and has been shown to significantly reduce mass loss in freeze–thaw cycles and limit microcracking [5]. Fibers help bridge cracks and enhance interlayer cohesion, impeding degradation along interfaces. Similarly, glass fibres have been successfully used to increase chloride resistance. They act as micro-reinforcement that restrains crack propagation and reduces pore connectivity, so printed concrete with fibres shows a lower chloride diffusion coefficient [6]. Beyond mix adjustments, proper curing of freshly printed elements is critical. Printed concrete should be protected immediately after deposition from rapid drying. External curing (e.g., covering with wet geotextile, misting the surface) or internal curing via superabsorbent polymers is recommended to minimize plastic shrinkage and early cracking [2]. It is also important to minimize interlayer delays and, where appropriate, mechanically treat the surface (e.g., light grinding or brushing/coating between layers) to improve bond. This reduces interface weakness and limits ingress along these pathways [2]. Some studies even discuss tailoring special geometries and hollow profiles in 3DPC that can better withstand environmental exposure (e.g., enabling more uniform drying or reducing self-stresses). Overall, a combination of a high-quality mix (with tailored formulation, SCMs, and fibres) and a controlled printing process (minimal porosity, adequate curing) can deliver highly durable 3D-printed concrete [7]. These principles aim to ensure that, despite its layered structure, 3DPC can reach durability comparable to conventional concrete and enable reliable use of 3D printing for long-lasting structural applications.

To delineate the scope of this work, the study first quantifies the influence of discrete fibre type - comparing steel and polyvinyl alcohol (PVA) fibres - on the durability-relevant behaviour of 3D-printed cementitious materials. Based on these results, PVA fibres are selected for a second experimental stage that investigates how post-printing curing regimes affect (i) freeze-thaw resistance (with and without de-icing salts), (ii) the rate of carbonation, and (iii) water permeability under pressure. This two-step design enables us to decouple material reinforcement effects from curing-related transport and degradation mechanisms, and to identify practical parameters with the greatest impact on service life.

2 Materials and Methods

2.1 Experimental design

The use of dispersed reinforcement has undeniable advantages in terms of mechanical properties of 3D printed material. Mechanical parameters depend on the material and geometry of the fibres. The fibre material has proven to be a crucial parameter, which in this case will positively affect the ductility of the material but may negatively affect the durability parameters. This work is divided into two phases. The first phase is focused on comparing the fibre material (steel vs. PVA), where the use of steel fibres was preferred in terms of their influence on the mechanical parameters of the 3D printed material. However, the results showed a very negative influence of steel fibres in terms of the material's resistance to freeze-thaw cycles in the presence of de-icing salts. The evaluation criterion was the limits given by the national standard ČSN P 73 2404 [17]. For this reason, the variant with PVA fibres was chosen,

where the material met the criterion but with the acceptance of a compromise variant with reduced mechanical properties.

In the second phase of the experimental program, the work focused on the effect of treatment of printed elements on resistance to freeze-thaw cycles in the presence of de-icing salts. In the laboratory, printed elements are commonly covered with PE foil to prevent water evaporation. It turned out that the time for which the elements are treated has a fundamental effect on durability parameters. During the production process of 3D printed elements, there is often pressure to ship as quickly as possible. However, our laboratory requires at least 3 days of treatment of elements to prevent excessive water evaporation and to achieve sufficient mechanical parameters. When evaluating the effect of treatment, the time of 3 days did not prove to be sufficient (failure to meet the limit according to ČSN P 73 2404 [17]), however, the authors' experience with the requirement of fast shipping led to the necessity of using this variant for performing other common durability tests (frost resistance without de-icing salts, carbonation rate, depth of penetration of water under pressure).

2.2 Materials, mixes, and printing

Five printable mixes were prepared (see Table 2). Fresh material bulk density was measured in accordance with ČSN EN 1015-6 [9] to verify the target composition before printing. Specimens were printed in layers using an extrusion-based gantry printer. After printing, specimens were cut to the dimensions required by each test method.

The produced mixes (see Table 2) in this study are based on research [11] and contained type II Portland cement 52.5 N (type CEM II/A-S according to EN 197-1), combination of natural quartz sand with maximum particle size of 1.25 mm, limestone filler, combination of ground quartz fillers and silica fume. The granulometry of the individual components is recorded on Fig. 1. A polycarboxylate-based superplasticizer (MasterGlenium ACE 300) was used to reduce water-binder ratio. All mixes also contained polypropylene fibres (~0.1% vol.). Polygalactomannan ether was used as a viscosity-modifying admixture (VMA).

Only some mixtures contained additives: a non-alkali setting accelerator (aqueous solution of aluminum sulphate, 75% water) was added to selected mixtures, and dispersed reinforcements were inserted into others – either steel fibres (brass coated, ~1.0% vol.) or PVA fibres (~0.25% vol.). The following Table 1 lists the material parameters of dispersed reinforcement specified by the manufacturer.

The experiment used a gantry printer suitable for printing cement material developed in the 3D Star project. The entire system consists of a mixer, pump, hoses, print head and end nozzle. The circular nozzle with a diameter of 20 mm was used in every cases. The average printing speed reached 100 mm per second. At this speed, the time gap between returning to the original position was minimal and there was no possible formation of a cold joints between successive layers.

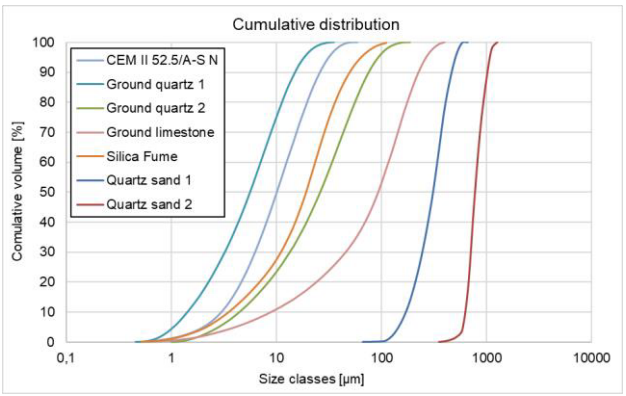

Fig. 1: The granulometry of the individual components.

Table 1: Material parameters of fibres.

Fibre type	Diameter	Length	Tensile strength	Density
	[mm]	[mm]	[MPa]	[kg.m^{-3}]
Steel fibres	0.20	14.0	2200	7850
PVA fibres	0.20	12.0	800	1300
PP fibres	0.03	5.0	420	910

Table 2: Materials composition in [kg.m^{-3}].

	REF	REF-ACC	SFIB	SFIB-ACC	PVA-ACC
CEM II/A-S 52.5 N	370	353	367	352	356
Ground quartz 1 (d50 = 6 μm)	188	179	186	179	181
Ground quartz 2 (d50 = 27 μm)	188	179	186	179	181
Ground limestone (d50 = 93 μm)	41	39	41	39	39
Silica fume (d50 = 21 μm)	94	90	93	89	90
Quartz sand 1: 0.10 – 0.63 mm	412	393	408	392	396
Quartz sand 2: 0.63 – 1.25 mm	589	562	584	560	567
5 mm PP fibres (d=30 μm)	1	1	1	1	1
Superplasticizer	25	24	25	24	24
VMA	2	2	2	2	2
Water	210	200	208	200	202
Steel fibres	0	0	79	76	0
PVA fibres	0	0	0	0	3
Setting accelerator	0	67	0	67	67

REF mixture - mixture without fibres, without setting accelerator
REF-ACC mixture - mixture without fibres, with setting accelerator
SFIB mixture - mixture with steel fibres, without setting accelerator
SFIB-ACC mixture - mixture with steel fibres, with setting accelerator
PVA-ACC mixture - mixture with PVA fibres, with setting accelerator

To determine the effect of curing type, elements with dimensions of 280×280×400 mm were printed (see Fig. 2). These elements were treated according to the procedure mentioned in chapter 2.3. After 28 days, 3 test specimens with dimensions of 150×150×30 mm (see Fig. 3) were prepared from each sample. Then the specimens were left in water at a temperature of 20 °C until full saturation.

Fig. 2: Printed elements.

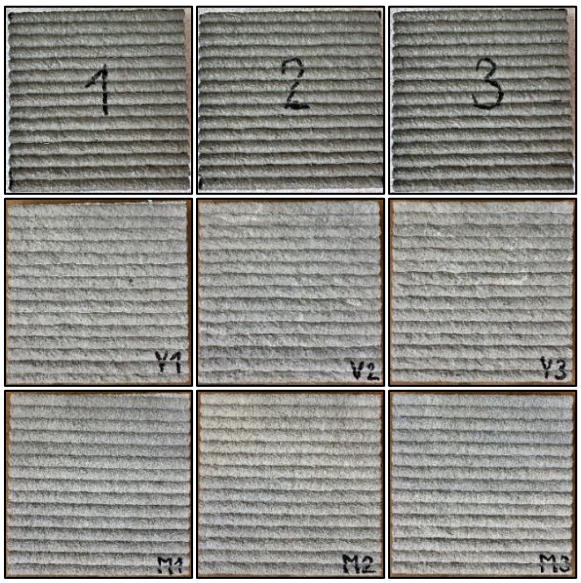

Fig. 3: Prepared test specimens before being placed in the climate chamber. (Curing type: 1-3: PE sheet 28d, V1-V3: PE sheet 3d, M1-M3: without PE sheet.).

A double wall measuring 1000×200×45 mm (see Fig. 4) was printed for the frost resistance test. From the previous experiment, it emerged that when printing this double wall, the printed layers were imperfectly connected. This created voids that could negatively affect the durability of such a printed element. For this reason, this element was selected as a suitable candidate for frost resistance testing. After printing, the sample was treated according to procedure 2) of chapter 2.3. After 28 days, 6 test specimens intended for freezing cycles with dimensions of 45×45×160 mm (see Fig. 5) and 3 reference specimens were prepared from the double wall sample. The test specimens were then left in water at 20 °C until fully saturated.

Fig. 4: The 3D printed double wall with imperfect connection.

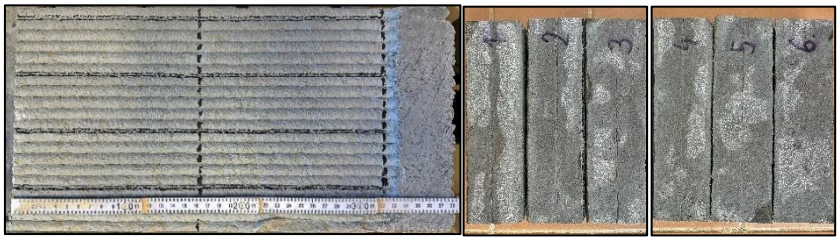

Fig. 5: The 3D printed double wall.

The durability test in stage one and some of the test in stage two were not performed on the specimens printed directly; instead, the fresh printable mix was conveyed through the same pump–hose–nozzle system used for printing and discharged into rigid molds, where it was manually compacted and surface-leveled to expel entrapped air and ensure a uniform test face (see Fig. 6). See details in section “Test methods”, where test specimens are defined for each test.

Fig. 6: Method of filling molds for some types of tests performed.

2.3 Specimen curing

For the steel-fibre series (stage one, assessment of fibre type), the printed elements were stored fully submerged in water at 20±2 °C from demoulding until the test age (28 days).

Curing regimes (applied to the PVA-reinforced mix in stage two) were selected to reflect practical post-printing scenarios. Before specimens were cut to test dimensions, the printed elements were subjected to one of three post-printing curing regimes:

1) Without PE sheet: left without sealing at 20±2°C, RH 55±5% until the 28-day test age.
2) PE sheet: immediately wrapped in impermeable polyethylene sheeting (PE sheet) for 3 days, then unwrapped and kept in air as 1) until the 28-day test age.

3) PE sheet until testing (28 days): immediately wrapped in impermeable polyethylene sheeting and kept sealed until the 28-day test age.

2.4 Test methods

All durability tests followed national or European standards as specified here. For each method, the primary response variables are listed; detailed parameters (cycle profiles, durations, exposure media) conformed to the cited standards.

2.4.1 Freeze–thaw with de-icing chemicals – ČSN 73 1326, Method C [10]

Freeze-thaw resistance with de-icing salts was evaluated in accordance with ČSN 73 1326, Method C. Specimens were placed in a climatic chamber with the tested surface continuously exposed to a 3% NaCl solution. Each thermal cycle comprised cooling from +5 °C to −18 °C in 30 min, holding at −18 °C for 150 min, heating back to +5 °C in 30 min, and holding at +5 °C for 150 min (total 6 h per cycle). After every 25 cycles, material scaled from the surface was rinsed/collected into a container, dried, and weighed; the result was normalized to 1 m² of exposed area ($kg \cdot m^{-2}$). The cumulative scaled mass per area was then compared with the acceptance limits specified in ČSN EN 206+A2 [16] and ČSN P 73 2404 [17] to assess compliance.

The test was performed on steel-fibre-reinforced specimens (stage one). These specimens were not printed directly; instead, the fresh printable mix was conveyed through the same pump–hose–nozzle system used for printing and discharged into rigid molds, where it was manually compacted and surface-leveled to expel entrapped air and ensure a uniform test face.

2.4.2 Freeze – thaw with de-icing chemicals – ČSN 73 1326, Method A [10]

Freeze-thaw resistance with de-icing salts was evaluated in accordance with ČSN 73 1326, Method A. Specimens were placed in a climatic chamber with the tested surface continuously exposed to a 3% NaCl solution. Each thermal cycle comprised cooling from +20 °C to −15 °C in 45 min, holding at −15 °C for 15 min, heating back to +20 °C in 45 min, and holding at +20 °C for 15 min (total 2 h per cycle). After every 25 cycles, material scaled from the surface was rinsed/collected into a container, dried, and weighed; the result was normalized to 1 m² of exposed area ($kg \cdot m^{-2}$). The cumulative scaled mass per area was then compared with the acceptance limits specified in ČSN EN 206+A2 [16] and ČSN P 73 2404 [17] to assess compliance.

The test was performed on PVA-fibre-reinforced specimens (stage two). The procedure was performed on a specimen cut from the 3D-printed element. The sample was sawn to the required dimensions.

2.4.3 Freeze–thaw without de-icing chemicals – ČSN 72 2452 [11]

Freeze-thaw resistance without de-icing salts was evaluated in accordance with ČSN 72 2452. Prismatic specimens were placed in a climatic chamber and subjected to repeated water–air cycles. Each cycle consisted of cooling from +20 °C to −20 °C in 15 min, holding at −20 °C for 240 min, heating back to +20 °C in 15 min, and holding at +20 °C for 120 min. During the heating phase, the chamber (and thus the specimens) was flooded with water at 20 °C to ensure saturated thawing. After every 25 cycles, degradation was quantified by mass loss determination and non-destructive measurement of the dynamic modulus of elasticity using an ultrasonic pulse method. The ultrasonic pulse method is a suitable method for detecting the formation of cavities or other internal damage (Abdulkareem et al., 2024) [19]. The durability was then assessed by (i) the ratio of flexural tensile strength of F-T cycled vs. referential companion specimens, or (ii) by the relative dynamic modulus; in both cases, the material is deemed F-T resistant up to the number of cycles at which the ratio remains ≥ 75 %. Tests are typically conducted to 100 cycles unless failure criteria are reached earlier.

The test was performed on PVA-fibre-reinforced specimens (stage two). The procedure was performed on a specimen cut from the 3D-printed element. The sample was sawn to the required dimensions.

2.4.4 Depth of penetration of water under pressure – ČSN EN 12390-8 [12]

Specimens were exposed to pressurised water at 0.5 MPa for 72 h. Subsequently, the specimens were split perpendicular to the pressurised face, and the maximum depth of water penetration was

measured from the exposed surface (mm). The result indicates resistance to pressurised water ingress for conformity/comparison purposes.

The test was performed on PVA-fibre-reinforced specimens (stage two). These specimens were not printed directly; instead, the fresh printable mix was conveyed through the same pump-hose-nozzle system used for printing and discharged into rigid molds, where it was manually compacted and surface-leveled to expel entrapped air and ensure a uniform test face.

2.4.5 Carbonation resistance (accelerated) – ČSN EN 12390-12 [13]

After curing, specimens are exposed in a controlled atmosphere (~3,5% CO_2, ~20 °C, ~65% RH) for a fixed duration. At specified ages (0, 7, 28 days), specimens are split, and the carbonation depth is measured on the fracture surface using phenolphthalein (mm). Results are reported as depth vs. time and, where required, as an apparent carbonation coefficient ($\sqrt{t}$ law) for comparison/conformity.

The test was performed on PVA-fibre-reinforced specimens (stage two). These specimens were not printed directly; instead, the fresh printable mix was conveyed through the same pump–hose–nozzle system used for printing and discharged into rigid molds, where it was manually compacted and surface-leveled to expel entrapped air and ensure a uniform test face. For comparison between the carbonation rate obtained by the accelerated method and the actual (natural) carbonation rate, printed specimens aged up to about 2 years were used.

2.4.6 Water absorption – ČSN 73 1316 [14]

The specimen is saturated in water at 20 ± 2 °C to a constant mass (recorded as the saturated mass), then dried at 105 ± 5 °C to a constant mass (the dry mass). Water absorption by mass is expressed as the percentage increase from m_d to m_s.

This method was used for all specimens (stage one and two).

2.4.7 Bulk density of hardened concrete – ČSN EN 12390-7 [15]

Bulk density was determined in both the oven-dry and fully saturated states. Specimens were first dried at 105±5 °C to constant mass and this mass was recorded as the dry mass. For the saturated state, specimens were water-saturated at 20±2 °C to constant mass. The specimen volume was obtained by hydrostatic weighing (weighing under water), i.e., from the difference between the mass in air and the apparent mass in water. Bulk density in the dry state (dry mass/volume) and in the saturated state (saturated mass/volume) were then calculated.

This method was used for all specimens (stage one and two).

For each test point, n ≥ 3 specimens were measured. Results in tables are reported as mean ± standard deviation (SD).

3 Results and Discussion

3.1. Freeze-Thaw durability test (method C) – stage one

The cyclic freeze-thaw resistance test in the presence of de-icing salts (ČSN 73 1326, Method C [10]) revealed pronounced differences among the individual mixes. The poorest performance was observed for the steel-fibre-reinforced material, which suffered the greatest areal loss of surface layers due to salt-scaling. After 75 freezing cycles, the steel-reinforced mix exhibited spalling of approximately 1100–1530 g/m², whereas the reference mix without fibres showed a loss of only 278 g/m² and the mix reinforced with PVA fibres 772 g/m². The presence of steel fibres therefore markedly reduces resistance to frost and salts, probably due to their corrosion. Corrosion products expand and induce additional cracking and detachment of the concrete cover. This surface degradation with corroding steel fibres is also evident visually (see Fig. 7). By contrast, in the mix with PVA fibres, which do not corrode and can bridge microcracks, the same test produced substantially less surface scaling. This result confirms that replacing steel reinforcement with dispersed PVA reinforcement significantly improved the material's frost resistance in a de-icing-salt environment.

Fig. 7: Specimens after 75 F-T cycles – method C
(From left to right: REF, REF-ACC, SFIB, SFIB-ACC).

Table 3: Surface scaling under freeze-thaw cycles (method C) with de-icing salts.

Mixture	Bulk density, saturated [kg.m^{-3}]		Bulk density, dried [kg.m^{-3}]		Water absorption [%]		Mass loss (surface scaling) – method C [g.m^{-2}]					
							25 cycles		50 cycles		75 cycles	
	Mean	SD	Mean	SD	Mean	SD	Mean	SD	Mean	SD	Mean	SD
REF	2150	12	2060	14	4.1	0.2	92	9	200	25	278	41
REF-ACC	2050	25	1910	22	7.4	0.4	428	61	566	103	608	138
SFIB	2190	18	2070	22	5.8	0.3	75	14	540	105	1106	189
SFIB-ACC	2150	27	1990	25	7.9	0.6	337	68	764	139	1532	291
PVA-ACC	2100	17	1940	19	8,5	0,3	129	16	504	78	772	127

For assessment under the applicable standards, the measured mass losses were compared with the limiting values for exposure classes XF according to the national application document to EN 206 (ČSN P 73 2404 [17]). After 50 cycles (exposure XF2 - moderate water saturation with de-icing salt), all test series met the requirement of max. 1500 g/m² (the highest loss was ~0.76 kg/m² for mix SFIB-ACC). However, after 75 cycles (exposure XF4 - high water saturation with de-icing salt, requirement max. 1000 g/m²), the steel-fibre mixes failed to meet this stringent limit—the recorded losses of ~1100 and 1500 g/m² for variants SFIB and SFIB-ACC exceeded it and thus did not satisfy the XF4 durability criteria. In contrast, the reference mixes (REF and REF-ACC) and the PVA-fibre mix (PVA-ACC) remained below 1000 g/m² and, after 75 cycles, complied with class XF4. Based on these results, the second phase of experiments discontinued testing with steel fibres and switched to PVA reinforcement. Steel fibres increased strength but at the cost of failing the frost-resistance requirement, whereas the PVA variant met the criteria (albeit with a slight strength compromise [16]).

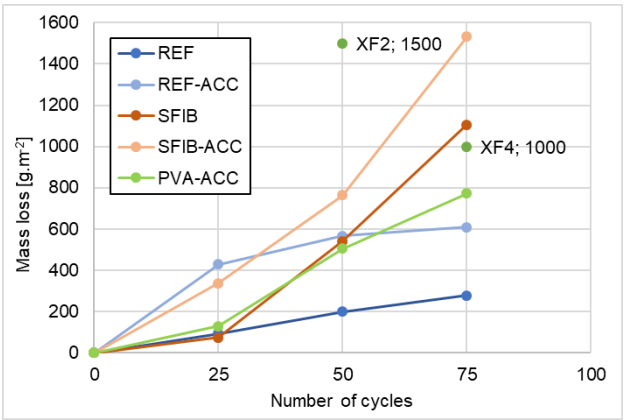

Fig. 8: Mass loss (ČSN 73 1326 - Method C) vs. No. of cycles + XF limits.

The results further show the effect of the set accelerator. Mixes with the accelerator (ACC) exhibited roughly double the water absorption compared to mixes without the admixture (e.g., REF-ACC ~7.4% vs. REF ~4.1%) as well as higher mass loss under frost–salt action. Increased absorption indicates a more open pore structure, which may explain the observed lower resistance of these mixes to freeze–thaw with salt. On the other hand, the applied accelerator dosage (see Table 2) was necessary to achieve the required printability of the fresh mix. Without acceleration the material would not meet the technological demands of 3D printing. These findings indicate that dispersed reinforcement and mix composition fundamentally affect the durability of printed material: steel fibres can cause premature

surface failure in an aggressive (saline) environment, whereas more suitable PVA fibres do not. At the same time, chemical admixtures necessary for printing worsen the microstructure and their negative impact needs to be mitigated by other measures.

The following test results were performed on a mixture labeled PVA-ACC, i.e. containing PVA fibres and a setting accelerator - stage two.

3.2. Freeze-Thaw durability test (method A) – stage two

In the second experimental phase, the same mix (PVA-ACC) was investigated under different curing conditions to assess the effect of additional curing on frost resistance. Specimens were exposed to cyclic freezing with a salt solution (ČSN 73 1326, Method A [10]) and compared after the standard 100 cycles. Extended curing had a dramatic positive effect: samples covered with PE film for 28 days showed a loss of only ~620 g/m² after 100 cycles, well below the 1000 g/m² limit required for the most stringent class XF4. By contrast, specimens cured for only 3 days or left uncured suffered much higher losses (1259 and 1550 g/m² after 100 cycles), i.e., more than twice that of the 28-day variant and clearly above the 1000 g/m² threshold. Differences were evident already after 75 cycles (corresponding to the milder class XF2). The well-cured sample (28 days) lost about 384 g/m², whereas 3-day curing led to a loss of 922 g/m² and no curing to 1065 g/m². Although all these values met the XF2 limit (1250 g/m² after 75 cycles per ČSN P 73 2404 [17]), the margin for the uncured variant was narrow. Conversely, the fully cured material retained a large safety margin even with respect to the strict XF4 classification (the 28-day variant comfortably met 1000 g/m² after 100 cycles). In terms of code criteria, only well-cured 3D-printed specimens satisfied the XF4 requirements (50-year service life under the most severe freeze–thaw exposure), whereas insufficiently cured variants do not meet these conditions and barely attain the XF2 level. These findings clearly show that proper curing is key to the long-term durability of 3D-printed concrete. Only by ensuring sufficient hydration and limiting early drying or shrinkage will the material maintain the necessary resistance to frost and de-icing chemicals. Figure 9 illustrates the surface condition after 100 cycles. The well-cured specimen shows minimal damage, while the uncured one exhibits severe degradation (scaled surface and exposed layers).

The curing mechanism is also related to the transport properties of concrete. Poorly cured elements exhibited substantially higher final water absorption. With 28-day film curing, absorption was ~7.7%, whereas the same mix cured for only 3 days increased to 11.5% and without curing to 13.2%. This increase in absorption with insufficient curing can be attributed to early shrinkage and microcracking in inadequately hydrated material. Microcracks increase pore connectivity and facilitate fluid ingress. The measured absorption values closely correlate with frost resistance. The variant with the lowest absorption (28-day curing, 7.7%) also had the smallest loss under freeze–thaw cycles (620 g/m²), whereas the highest absorption (no curing, 13.2%) corresponded to the greatest loss (1550 g/m²). It follows that thorough curing reduces open porosity and limits microcrack formation, thereby improving resistance to water penetration and subsequent freeze–thaw damage. While absorption alone does not unambiguously determine durability, the consistent coincidence of higher absorption with greater freeze damage confirms the importance of a quality curing process for 3D-printed concrete elements.

Table 4: Surface scaling under freeze-thaw cycles (method A) with de-icing salts.

Curing Type	Bulk density, saturated [kg.m^{-3}]		Bulk density, dried [kg.m^{-3}]		Water absorption [%]		Mass loss (surface scaling) – method A [g.m^{-2}]							
	Mean	SD	Mean	SD	Mean	SD	25 cycles		50 cycles		75 cycles		100 cycles	
							Mean	SD	Mean	SD	Mean	SD	Mean	SD
PE sheet for 28 days	2150	18	1990	21	7.7	0.3	90	17	198	34	384	69	620	106
PE sheet for 3 days	2130	21	1910	24	11.5	0.5	249	51	521	94	922	152	1259	194
No PE sheet	2100	24	1860	19	13.2	0.6	422	89	602	98	1065	207	1550	273

Fig. 9: Specimens after 100 F-T cycles – method A
(From left to right: PE sheet 28d, PE sheet 3d, No PE sheet).

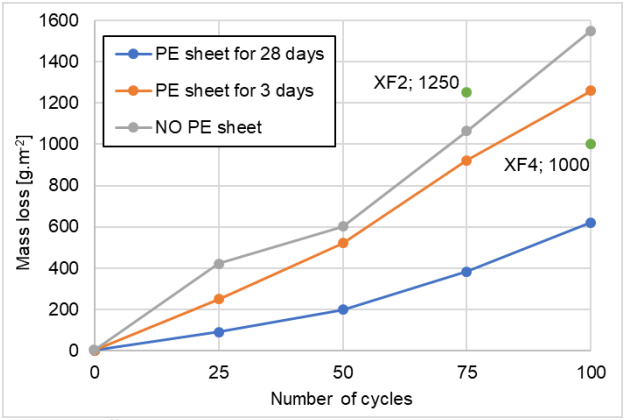

Fig. 10: Mass loss (ČSN 73 1326 - Method A) vs. No. of cycles + XF limits.

3.3. Freeze-Thaw durability test (printed prismatic specimens) – stage two

To verify frost resistance in an environment without chemical de-icers, a cyclic freezing test in water was performed in accordance with ČSN 72 2452 [11]. The test was carried out on prismatic specimens printed as a double wall (two parallel thin walls of PVA-ACC material printed side by side). After 100 freeze cycles (in water), there was no measurable surface mass loss, confirming that without salts the surface does not exhibit scaling as in the previous tests. However, visible delamination cracks at the interlayer interface appeared in half of the specimens. Specifically, the connecting web between the two printed walls separated (see Fig. 11). Despite these defects, the overall static function of the elements was largely preserved. The average flexural strength after the freeze test reached about 85% of the strength of the reference (non-cycled) specimens, exceeding the minimum requirement of 75% set by ČSN 72 2452 [11] for frost resistance. The relative dynamic modulus of elasticity remained at ~99% of the original value after 100 cycles, also well above the 75% criterion. The printed PVA-ACC material can therefore be rated as frost-resistant under ČSN in environments without de-icing salts, as it retained sufficient strength and stiffness. It should be noted, however, that the identified interlayer cracks may represent the onset of layered-structure failure. Although in this test the resulting delamination had no major effect on load-bearing capacity (the fracture during bending propagated along other paths - see Fig. 12), they could progress over the long term and threaten element integrity. From a practical standpoint, it is thus desirable to improve interlayer bond during printing to minimize the occurrence of such defects in the future.

Table 5: Freeze-thaw resistance test results according to ČSN 72 2452 [11].

Parameter	**Bulk density, saturated**	**Flexural strength (3-point bending)**	**Freeze–thaw resistance coefficient**	**Relative dynamic modulus of elasticity after 100 F-T cycles**	**Visual assessment after 100 F-T cycles**
	[kg.m^{-3}]	**[MPa]**	**[%]**	**[%]**	
After 100 F-T cycles				After 100 F-T cycles	
Mean	2140	8.6		98.8	
SD	26	1.0	85	0.7	
Reference					
Mean	2090	10.1		-	

SD	6	0.7			walls (double-wall interface).

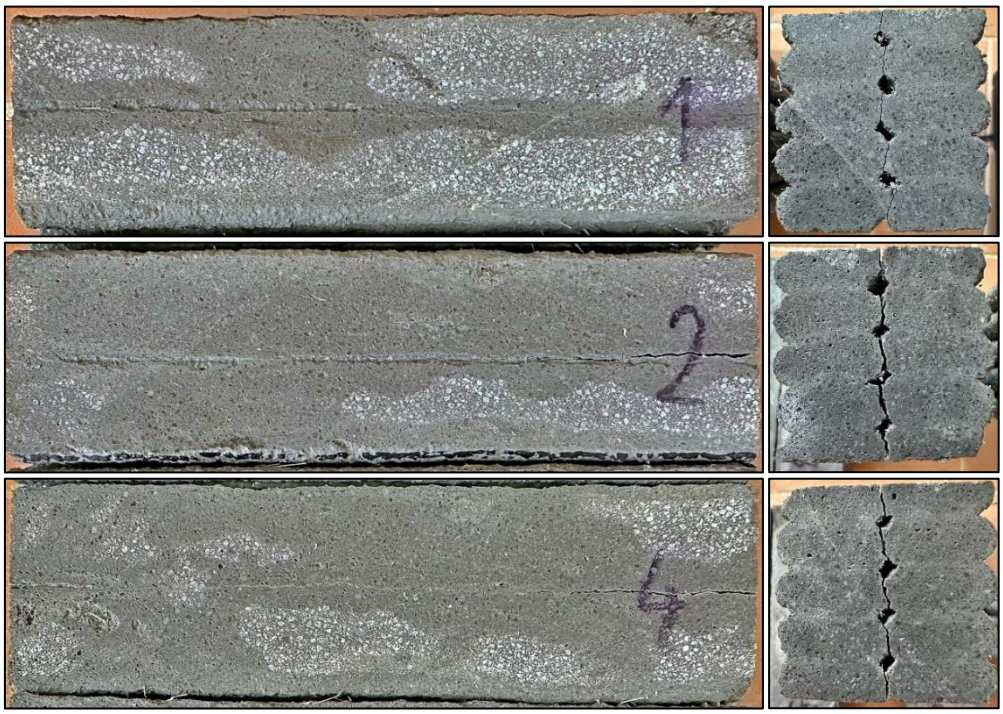

Fig. 11: Specimens after 100 F-T cycle: The crack between the two walls.

Fig. 12: Flexural test - failure mode.

3.4. Carbonation rate test – stage two

Carbonation rate, K_{AC}, was determined from the linear relationship between mean carbonation depth and the square root of exposure time. For each specimen series, the mean depth d_k was measured at t = 0, 7, and 28 days. The intercept point a was taken directly from the t=0 measurement (initial carbonation depth). The three data points $d_k(t)$ were then regressed against square root of t to obtain a best-fit line:

$$d_k = a + K_{AC}\sqrt{t} \quad (1)$$

The slope equals K_{AC} (units: mm·day^{0,5}). In accordance with the standard, we required a coefficient of determination $R^2 \geq 0.95$. This procedure yields a single K_{AC} value for defined curing/mixture condition during the test and does not describe the actual rate of carbonation in a common environment.

Fig. 14 illustrates test specimens that were stored in a chamber with a CO_2 concentration of approximately 3.5% vol. The parameters of equation (1) were determined from the average values of the carbonation depth (see Fig. 13):

a = 0.325 mm
K_{AC} = 1.4583 mm·day^{0,5}
R^2 = 0.9831

In the graph in Fig. 15, this relationship is plotted with the curve labeled “Model EN 12390-12”.

To verify and refine the carbonation rate model, old samples that were stored in the laboratory archive in a normal laboratory environment were subjected to a carbonation depth test using phenolphthalein solution (see Fig. 16). The actual measured carbonation values at a given age of the samples are recorded in Table 6. The values are plotted in the graph in Fig. 15 under the label "Measured values".

For a simple fitting of the actual carbonation depth and the carbonation depth over time obtained by the accelerated method, the coefficient C was introduced. The coefficient C in our case is equal to 0.24. It is necessary to mention that the results obtained by the accelerated carbonation method are highly related to the type of material and the conditions of treatment and testing. The authors of this work did not aim to present a general equation for the carbonation rate for 3D printing materials. The following equation (2) describes the behaviour of one specific type of material with respect to the carbonation depth over time:

$$d_{k,actual} = a + C.K_{AC}\sqrt{t} \tag{2}$$

The reduced model (2) with the C value is shown in the graph in Fig. 15 as "Proposed model" and satisfactorily predicts the carbonation depth value over time for this specific material. The curve given by this model overlaps with the carbonation depth values measured on the printed elements while considering a certain measurement uncertainty defined by the standard deviation.

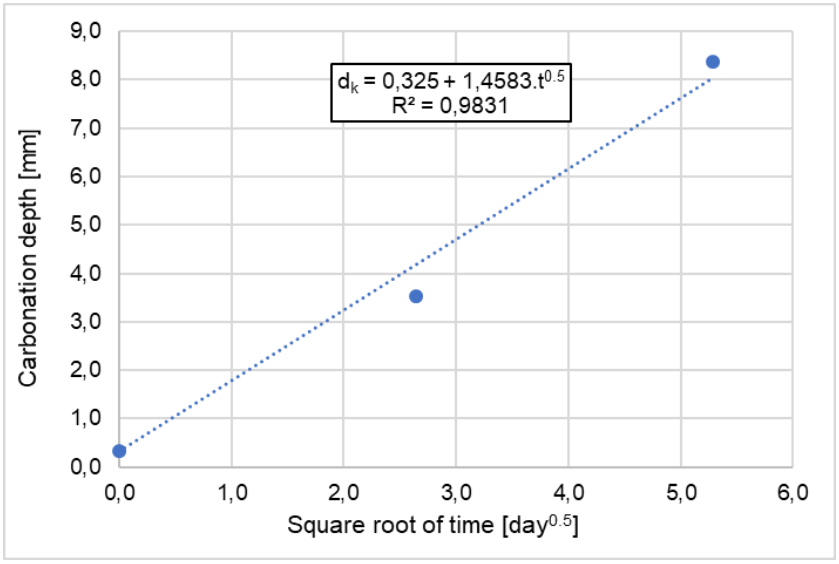

Fig. 13: Determination of carbonation rate.

Fig. 14: Test specimens (From left to right: 7 days and 28 days in CO_2 chamber).

Table 6: Carbonation depth over time.

Age [day]	Parameter	30	161	349	458	675
Carbonation depth [mm]	Mean	2.9	4.4	7.3	7.6	8.8
	SD	1.5	1.5	0.9	1.1	0.8

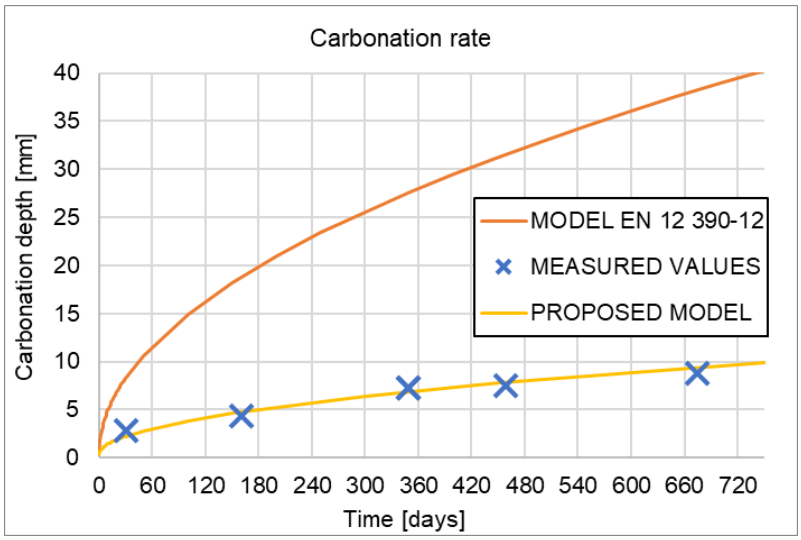

Fig. 15: Carbonation rate

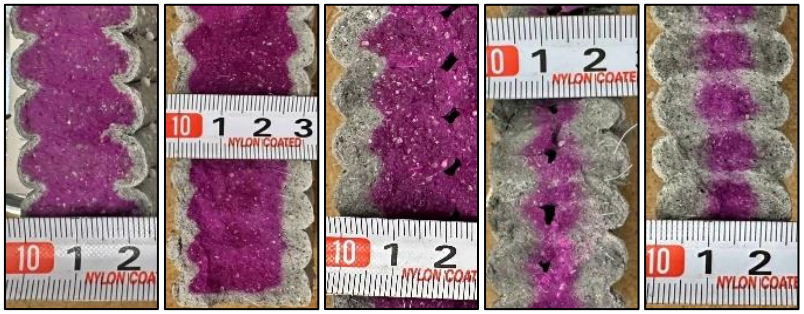

Fig. 16: Carbonation depth, (From left to right: 30, 161, 349, 458 and 675 days old specimen).

3.4.1 Carbonation Depth vs. Standard Cover Requirements

Table 5 shows that after 675 days of exposure (nearly two years), the 3D-printed concrete walls reached a maximum carbonation depth of 8.8 mm. This measured carbonation depth is well within the protective concrete cover typically provided for steel reinforcement. According to the draft ICC standard for 3D-printed wall systems (Table 403.7) [18], the minimum concrete cover for reinforcement is as follows:

19 mm (¾ inch) for reinforcement not exposed to weather (e.g. interior conditions).

38 mm (1½ inches) for reinforcement exposed to weather or ground (for smaller bars, No. 5 and below), and 50 mm (2 inches) for larger bars in exposed conditions.

Even after nearly two years, the carbonation front (8.8 mm) does not approach these cover thicknesses. In other words, the depth of carbonated concrete is less than half of the smallest required cover (19 mm for interior steel), and is far below the 38–50 mm cover mandated for reinforcement in exterior exposure. The standard cover provides a substantial buffer, and the observed carbonation depth does not exceed any code-prescribed cover limit at this age. Therefore, no increase in the printed wall thickness (beyond the standard cover) is required for carbonation protection in this scenario. The existing cover thickness is sufficient to keep the reinforcement in an alkaline, non-carbonated zone after two years of exposure, meaning the 3D-printed wall meets durability expectations with regard to carbonation.

In the long term, using equation (2), it can be assumed that a carbonation depth of 19 mm will be achieved when the material is 8 years old and a carbonation depth of 38 mm when it is 31 years old (see Table 7). It is important to mention that the aforementioned document makes assumptions about the total width of the sample layer in terms of the necessary coverage of the steel reinforcement. However, it is clear that in such thin walls (up to 25 mm thick) as those printed in this study, conventional steel reinforcement cannot be placed effectively at all - such subtle elements must be designed either without reinforcement or with consideration for rapid carbonation of the entire cross-section.

Table 7: Predicted carbonation depth over time.

Age	**[year]**	1	2	4	6	8	10	20	30	40	50
Carbonation depth	**[mm]**	7.0	9.8	13.7	16.7	19.2	21.5	30.2	36.9	42.6	47.6

For long-term control of 3D printed elements in terms of the effect of carbonation on steel reinforcement, it is necessary to design a verification method. The non-destructive method proposed in the work by Flores-Nicolás et al., 2025 [20], using electrochemical noise measurement, appears to be optimal and should be considered in the subsequent stage of experimental investigation of the effect of carbonation.

3.5 Depth of penetration of water under pressure test – stage two

The final durability aspect assessed was water transport and material watertightness. The differences in absorption underscore the importance of mix composition and curing. The presence of the accelerator and insufficient curing increase the matrix's overall absorption, which is related to higher permeability to water and aggressive media. For a quantitative assessment of watertightness, the depth of water penetration under pressure (ČSN EN 12390-8 [12]) was tested on cubic specimens made from mix PVA-ACC. The test specmens (150 mm cubes) were prepared in the standard way from fresh mix. Subsequent curing followed the PE-3d regime (covered with film for 3 days, then air-cured), analogous to the actual printed walls. The measured water penetration depth (pressure 0.5 MPa for 72 hours) was 20 mm for 3-day specimens, ~26 mm for 7-day, and ~29 mm for 28-day specimens. The values increased slightly with time, which can be attributed to curing being discontinued after 3 days. Later, specimens may have developed shrinkage microcracks that allowed somewhat deeper water ingress. For comparison with code requirements, the results were compared with the limiting values for environmental classes according to Table F1.1 of ČSN P 73 2404 [17]. In all common exposure classes (XC - carbonation, XD - chlorides, XF - freeze–thaw, XA1–XA2 - mild chemical attack), the measured penetration depths satisfied the corresponding limits. These range from 35–50 mm, so our material with a maximum penetration of ~29 mm met these requirements with margin. Only in the case of the most aggressive chemical environment XA3 was the 20 mm limit exceeded (~29 mm at 28 days), meaning that for structures exposed to strongly acidic environments this mix would not meet watertightness requirements. It must be emphasized, however, that the laboratory test on cast specimens may not fully capture the layered structure of 3D printing. Visual inspection revealed that printing defects (e.g., voids or discontinuous layers) can act as channels through which water penetrates much deeper. Fig. 17 schematically shows, on the right, a case of penetration reaching much deeper into the specimen along an insufficiently mixed setting accelerator layer. These anomalous cases were not included in the calculation of the average value (defective specimens were replaced by new measurements), but in engineering practice they represent a warning. If interlayer bonding is poor or cavities remain in the printed wall, water may locally penetrate much deeper than would be expected from an otherwise high-quality matrix. Overall, the printed mix PVA-ACC exhibits very good resistance to water penetration (comparable to conventional structural concrete) and meets national watertightness standards for most exposure conditions. Nevertheless, in view of its layered nature, quality control of the printing process is essential. Especially ensuring interlayer cohesion and minimizing defects that could create preferential pathways for water ingress. This is particularly important for thin-walled elements, where local penetration could jeopardize the durability of the entire cross-section.

Table 8: Depth of penetration over time.

Material age [days]	**Bulk density [kg.m^{-3}]**		**Depth of penetration [mm]**	
	Mean	**SD**	**Mean**	**SD**
3	1920	7	23	9.4
7	1910	10	26	19.4
28	1890	16	29	7.4

Table 9: Depth of penetration limits.

Exposure class	**XC4**	**XD2**	**XD3**	**XF1**	**XF2**	**XF3**	**XF4**	**XA1**	**XA2**	**XA3**
Max. depth of penetration [mm]	50	50	35	50	50	35	35	50	35	20

Fig. 17: Depth of penetration of water under pressure.

4 Conclusion

In conclusion, the durability performance of 3D-printed cementitious composites was found to depend strongly on mixture design, fibre reinforcement, and curing regime. The experimental results highlight several key findings:

• Steel fibre reinforcement significantly undermined freeze–thaw durability in the presence of de-icing salts, whereas adding PVA fibres does not have such a negative effect. Steel-fibre specimens suffered severe surface scaling and failed stringent frost-resistance criteria (attributed to fibre corrosion and induced cracking). In contrast, PVA-fibre specimens exhibited substantially less scaling and maintained compliance with required frost durability standards.

• Prolonged curing greatly improved durability indicators, while insufficient curing led to poor performance. 3D-printed samples that were properly cured (e.g. 28 days under protective cover) showed minimal surface scaling in freeze–thaw tests and lower water absorption, comfortably meeting high-level durability classes. By comparison, specimens cured only briefly (a few days) had markedly higher open porosity and absorption, translating to over twice the mass loss under freeze-thaw cycling. These results underscore that adequate curing (ensuring continued hydration and reducing early-age drying) is critical for long-term durability of printed concrete.

• The printed material demonstrated moderate carbonation rates and good resistance to water ingress. After nearly two years of natural exposure, carbonation depth remained below ~9 mm, well within typical concrete cover for reinforcement, indicating no early risk to embedded steel. Likewise, under pressurized water testing, the depth of penetration (roughly 20–30 mm at 0.5 MPa for 72 h) satisfied relevant code limits for watertightness in common exposure classes. These observations suggest that, with an optimized mix and curing regime, 3D-printed concrete can achieve comparable carbonation resistance and permeability to conventional vibrated concrete.

• The layered printing process introduces interlayer interfaces that can act as weak planes for durability. Evidence of degradation was often localized along horizontal layer boundaries – for example, freeze-thaw cracking tended to initiate at the interlayer zones, where bond quality and density were lower. Similarly, any printing defects or voids at interfaces provided preferential pathways for deeper water penetration. This anisotropic behaviour highlights the need for careful control of interlayer adhesion and uniformity in 3D-printed structures, as well as potential benefits of fibre reinforcement in bridging layer interfaces.

The findings of this study emphasize practical measures to ensure the durability of 3D-printed concrete in structural applications. Replacing corrosion-prone steel fibres with non-corrosive alternatives (like PVA), enforcing sufficient curing periods, and improving interlayer bond quality all serve to significantly enhance frost resistance, impermeability, and carbonation protection in printed elements. By adopting these measures, engineers can confidently extend the service life of 3D-printed cementitious structures. Moreover, the insights gained here inform future research and standards development, guiding the optimization of materials and printing processes to achieve reliable, long-term performance in emerging additive construction technologies.

Acknowledgement

This work was supported by The Technology Agency of the Czech Republic, grant FW06010422.

References

[1] MOUSAVI, M., RANGARAJU, P. (2025). Freeze–Thaw Durability of 3D Printed Concrete: A Comprehensive Review of Mechanisms, Materials, and Testing Strategies. CivilEng, 6(3), 47. https://doi.org/10.3390/civileng6030047

[2] VAN DER PUTTEN, J. - DE VOLDER, M. - VAN DEN HEEDE, P. - DEPREZ, M. - CNUDDE, V. - DE SCHUTTER, G. - VAN TITTELBOOM, K.: Transport properties of 3D printed cementitious materials with prolonged time gap between successive layers. Cement and Concrete Research, Vol. 155, 2022, 106777, https://doi.org/10.1016/j.cemconres.2022.106777

[3] ZHANG, Y. – QIAO, H. – QIAN, R. – XUE, C. – FENG, Q. – SU, L. – ZHANG, Y. S. – LIU, G. – DU, H.: Relationship between water transport behaviour and interlayer voids of 3D printed concrete. Construction and Building Materials, Vol. 326, 2022, 126731, https://doi.org/10.1016/j.conbuildmat.2022.126731

[4] LER, K. -H., MA, C. -K., CHIN, C. -L., IZNI SYAHRIZAL IBRAHIM, KHAIRUL HAZMAN PADIL, MOHD AMINUL IZMEER AB GHAFAR, & ALVA AMI LENYA. (2024). Porosity and durability tests on 3D printing concrete: A review. Construction and Building Materials, 446, 137973-137973. https://doi.org/10.1016/j.conbuildmat.2024.137973

[5] SRINIVAS, D., PANDA, B., SURANENI, P., & T. G. SITHARAM. (2025). Mix design optimization of 3D-printed cementitious composites for marine applications: Impact of binder composition, accelerated carbonation, and PVA fibers on strength and durability. *Construction and Building Materials*, *489*, 142389-142389. https://doi.org/10.1016/j.conbuildmat.2025.142389

[6] DU, L., ZHOU, J., LAI, J., WU, K., YIN, X., & HE, Y. (2023). Effect of pore structure on durability and mechanical performance of 3D printed concrete. Construction and Building Materials, 400, 132581-132581. https://doi.org/10.1016/j.conbuildmat.2023.132581

[7] NODEHI, M. - AGUAYO, F. - NODEHI, S. E. - GHOLAMPOUR, A. - OZBAKKALOGLU, T. - GENCEL, O.: Durability properties of 3D printed concrete (3DPC). Automation in Construction, Vol. 142, 2022, 104479, https://doi.org/10.1016/j.autcon.2022.104479

[8] VAN TITTELBOOM, K., MOHAN, M. K., SAVIJA, B., KEITA, E., MA, G., DU, H., KRUGER, J., CANEDA-MARTINEZ, L., WANG, L., BEKAERT, M., WANGLER, T., WANG, Z., MECHTCHERINE, V., ROUSSEL, N. On the micro- and meso-structure and durability of 3D printed concrete elements. Cement and Concrete Research. 2024, 185, 107649, https://doi.org/10.1016/j.cemconres.2024.107649

[9] ZHOU, L., GOU, M., JI, J., HOU, X., ZHANG, H. Durability and hardened properties of 3D printed concrete containing bauxite tailings. Materials Today Sustainability. 2024, 25, 100704, https://doi.org/10.1016/j.mtsust.2024.100704

[10] SKRIPKIŪNAS, G., TOLEGENOVA, A., RISHKO, L., AKMALAIULY, K., BALTUŠKIENĖ, D. Durability and Cracking Defects in 3D-Printed Concrete. Advances in Civil Engineering. 2025, Article ID 8592029, 8 p, https://doi.org/10.1155/adce/8592029.

[11] CITEK, D., HURTIG, K., KOLISKO, J, & KOTES, P., Cementitious Material Development for Additive Fabrication. MM Science Journal, 2024, https://doi.org/10.17973/MMSJ.2024_06_2024040

[9] ČSN EN 1015-6+A1 (72 2583): Metody zkoušení malt pro zdivo – Část 6: Stanovení objemové hmotnosti čerstvé malty. Praha: ÚNMZ / Česká agentura pro standardizaci, 2007, 16 s. (EN: Methods of test for mortar for masonry – Part 6: Determination of bulk density of fresh mortar.)

[10] ČSN 73 1326 (73 1326): Stanovení odolnosti povrchu cementového betonu proti působení vody a chemických rozmrazovacích látek. Praha: Česká agentura pro standardizaci, 1985. (Změna Z1: 2003.) (EN: Testing concrete – Resistance of concrete surface to de-icing chemicals.)

[11] ČSN 72 2452 (72 2452): Zkouška mrazuvzdornosti malty. Praha: ÚNMZ, 1968. Změna Z1: 2005. (EN: Testing of mortar — Frost resistance test.)

[12] ČSN EN 12390-8:2019: Zkoušení zatvrdlého betonu – Část 8: Hloubka průsaku vody pod tlakem. Praha: Česká agentura pro standardizaci (ČAS), 2019. (EN: Testing hardened concrete – Part 8: Depth of penetration of water under pressure.)

[13] ČSN EN 12390-12:2020: Zkoušení zatvrdlého betonu – Část 12: Stanovení potenciální odolnosti betonu proti karbonataci – Zrychlená metoda karbonatace. Praha: Česká agentura pro standardizaci (ČAS), 2020. (EN: Testing hardened concrete – Part 12: Determination of the potential carbonation resistance of concrete – Accelerated carbonation method.)

[14] ČSN 73 1316 (73 1316): Stanovení vlhkosti, nasákavosti a vzlínavosti betonu. Praha: ÚNMZ, 1990 (vydána 02/1990; zrušena 01.12.2003). (EN: Testing of concrete – Determination of moisture content, absorptivity and capillarity of concrete.)

[15] ČSN EN 12390-7:2019: Zkoušení zatvrdlého betonu – Část 7: Objemová hmotnost zatvrdlého betonu. Praha: Česká agentura pro standardizaci (ČAS), 2019. (EN: Testing hardened concrete – Part 7: Density of hardened concrete.)
[16] ČSN EN 206+A2:2021: Beton – Specifikace, vlastnosti, výroba a shoda. Praha: Česká agentura pro standardizaci (ČAS), 2021. (EN: Concrete – Specification, performance, production and conformity.)
[17] ČSN P 73 2404:2024 (ed. 2): Beton – Národní aplikační dokument k ČSN EN 206 (požadavky a postupy pro podmínky ČR). Praha: Česká agentura pro standardizaci (ČAS), 2024. (EN: Concrete – National application document to EN 206 (requirements and procedures for the Czech Republic).)
[18] INTERNATIONAL CODE COUNCIL (ICC): Standard for Automated Construction Technology for 3D Printing Walls — Public Draft (Public Comment Version). Washington, DC: ICC, 2025. (Table 403.7.1: Minimum Concrete Cover for Reinforcement.)
[19] ABDULKAREEM, O. M., ALSHAHWANY, R. B., SHLLA, R. D., AHMED, A. S., Performance of zero-slump concrete made with recycled concrete aggregate. Civil and Environmental Engineering. 2024, 20, 471–480, https://doi.org/10.2478/cee-2024-0036
[20] FLORES-NICOLÁS, A., FLORES-NICOLÁS, M., MENCHACA-CAMPOS, E. C., URUCHURTU-CHAVARÍN, J. Study on corrosion of reinforced concrete with synthetic fibre using electrochemical noise technique. Civil and Environmental Engineering. 2025, 21(1), 271–281, https://doi.org/10.2478/cee-2025-0021